Original Article

Tetrahedral DNA Nanostructure-modified Gold Nanorod-based Anticancer Nanomaterials for Combined Photothermal Therapy and Chemotherapy*

WU Hao[1,2], XU Jiang Shan[3], LI Yan Hong[4], WU Xing Han[4], HU Wei[2], LIU Meng Die[1,2], SUN Qiang[5,#], and GUO Bin[2,#]

1. Medical School of Chinese PLA, Beijing 100853, China; 2. Department of Stomatology, the First Medical Centre, Chinese PLA General Hospital, Beijing 100853, China; 3. College of Biomedical Engineering, Sichuan University, Chengdu 610064, Sichuan, China; 4. Institute of Medical Laboratory Animal Science, CAMS&PUMC, Beijing 100021, China; 5. State Key Laboratory of Oral Disease, National Clinical Research Center for Oral Diseases, West China College of Stomatology, Sichuan University, Chengdu 610064, Sichuan, China

Abstract

Objective To develop an effective treatment strategy to simultaneously avoid fatal adverse effects in the treatment of oral cancer, combination therapy has been explored because of its multiple functions. This work aims to develop a novel type of gold-nanorod-based nanomaterials decorated with tetrahedral DNA nanostructures (TDN) carrying antitumor drugs, namely, GNR@TDN-DOX nanocomposites.

Methods In the designed structure, TDN, with a three-dimensional geometry composed of DNA strands, can provide GC base pairs for binding with the anticancer drug doxorubicin (DOX). The photothermal heating properties, biocompatibility properties, and antitumor performance of obtained GNR@TDN-DOX nanocomposites were investigated to assess their application potential in tumor treatment.

Results Systematic studies have shown that the obtained GNR@TDN-DOX nanocomposites have high photothermal conversion under the illumination of an 808-nm infrared laser, leading to effective antitumor applications. In addition, the cell viability study shows that GNR@TDN-DOX nanocomposites have good biocompatibility. *In vitro* studies based on A375 cells show that the GNR@TDN-DOX nanocomposites can effectively eliminate cancer cells because of the combination of photothermal therapy induced by GNRS and chemotherapy induced by TDN-carrying DOX. The result shows that the obtained GNR@TDN-DOX nanocomposites have efficient cellular uptake and lysosome escape ability, together with their nuclear uptake behavior, which results in a significant antitumor effect.

Conclusion This work has demonstrated a potential nanoplatform for anticancer applications.

Key words: Nanomaterials; DNA tetrahedron; Gold nanorod; Combination therapy

Biomed Environ Sci, 2022; 35(12): 1115-1125 doi: 10.3967/bes2022.141 ISSN: 0895-3988

www.besjournal.com (full text) CN: 11-2816/Q

INTRODUCTION

Oral cancer, which occurs in oral cavities such as the tongue, gingiva, bucca, palate, and lip, ranks sixth among the most common cancer types worldwide[1], leading to nearly 180,000 deaths every year[2]. Traditional treatment strategies for oral cancer include surgical removal, radiotherapy, and chemotherapy[3]. In the past years, surgery and radiotherapy are still

*This work was supported by the 13th Five-year Plan for key Discipline Construction Project of PLA [A350109].

#Correspondence should be addressed to GUO Bin, Professor, E-mail: guobin0408@126.com, Tel: 86-10-66937964; SUN Qiang, Professor, E-mail: qiangsun@scu.edu.cn, Tel: 86-28-85503465.

Biographical note of the first author: WU Hao, male, born in 1988, Master, majoring in stomatology.

regarded as the major therapeutic modalities for oral cancer treatment, considering the limited effects of antineoplastic drugs. However, these methods can lead to observable facial defects and scars, radioactive bone necrosis, microbial infection, facial nerve palsy, trismus, and other related issues, which can cause great pain to patients. Notably, with the development of nanotechnology, a series of nanomaterials has been explored to eliminate oral tumors using photodynamic, photothermal therapy (PTT), and gene therapy, which are regarded as gentle therapies without serious adverse effects[4-6]. Among these pathways, PTT can kill cancer cells with rapidly increased temperature *via* harvesting laser energy. Notably, with a light source targeting the tumor site, PTT can significantly reduce damage to the adjacent normal tissues and apoptosis of normal cells[7]. In the past years, nanomaterials, namely, nanomedicines, such as precious metals[8,9], metal chalcogenides[10], carbon nanotubes[11,12], and their derivatives, have been well studied for their potential applications in PTT. Among these nanomaterials, gold nanostructures[9,13,14] have attracted great attention because of their ability to convert light into heat by absorbing light in the near-infrared (NIR) range, promoting the maximized penetration depth into animal issues. Moreover, by modulating the geometry and size of gold nanostructures, their absorbance peaks can be facilely tuned[15,16], which can provide more freedom for the development of novel nanomedicines.

Gold nanorods (GNRs), with a large length-to-diameter ratio, have particular longitudinal surface plasmon resonances, well-controlled morphology, and high-efficiency photothermal conversion ability[9,13,15]. In functionating GNRs and enhancing their ability to load and deliver anticancer drugs, great endeavors have been committed, such as applying cetyltrimethylammonium bromide and polyethyleneimine to modify the surfaces of GNRs and further linking with drugs[17]. Based on the objects linked, this strategy can combine several anticancer mechanisms and enhance the efficiency of killing cancer cells. For example, Ding et al.[18] reported an sgRNA/Cas9 complex nanoplatform for targeted gene editing and combined tumor therapy. Given the cell-targeting aptamer, nuclear targeting peptide, gene editing, and PTT agents, a remarkable antitumor effect was observed. Therefore, in this work, in achieving a novel nanomaterial based on GNRs for the combined therapy of oral cancer, it was proposed that tetrahedral DNA nanostructures (TDN) can be a potential media nanomaterial for the modification of GNRs[19-23]. TDN is a tetrahedral wireframe nanostructure assembled by four oligonucleotide-based base complementary pairing principles, which have been known for their biosafety, cellular internalization, and facile editing[24-28]. Notably, TDN can effectively bind to a series of medicine through incubation, molecular design, and chemical bonding. For example, TDN can load wogonin through hydrogen bonding between the hydroxyl groups of wogonin and the guanine and cytosine residues[29]. In addition, Lin et al.[24] developed a novel HApDC (HApt-TDN@DM1) drug-based TDN for HER2-positive breast tumors, which can target the HER2 protein and deliver chemotherapeutic drugs into tumor cells. Previous studies show that TDN can carry up considerable amount of doxorubicin (DOX) molecules through facile incubation and result in a series of benefits, particularly in cellular uptake and drug release[30]. In this regard, considering the effects of DOX in inhibiting topoisomerase II within the nucleus and intercalating into DNA to trigger cell apoptosis, the use of DOX-loaded TDN can be a potential component for the development of future anticancer drugs.

In this work, a new strategy to construct nanomaterials for PTT and combined chemotherapy was proposed, which can be potentially applied in the treatment of oral cancer. First, TDN-DOX nanocomposites by tight binding between DOX and DNA strands was synthesized and then decorated them onto the surface of PEG-modified GNRs, namely, GNR. Consequently, the multifunctional nanoplatform for cancer treatment was successfully obtained, which comprised GNRs as the photothermal agents and TDN-loading DOX as the chemotherapeutic drugs, based on the detailed characterization and analysis (the key synthesis steps of GNR@TDN-DOX and its antitumor mechanism are shown in Figure 1). The cell viability test on L929 cells suggests that the obtained GNR@TDN-DOX nanocomposites have good biocompatibility because of their unique structural design. *In vitro* cell study on A375 cells shows that biocompatible GNR@TDN-DOX nanocomposites have a significant antitumor effect because of the combination of PTT induced by GNRs and chemotherapy induced by the delivered antitumor drug DOX. Moreover, the obtained GNR@TDN-DOX nanocomposites have efficient cellular uptake, nuclear uptake, and lysosomal escape abilities, which result in the enhanced antitumor effect. Based on the results and analysis, this novel nanomaterial can provide a new strategy

for combination cancer therapy, which can also be applied to other diseases.

MATERIALS AND METHODS

Materials

All chemicals and solvents applied in this work were of analytical grade. DNA oligos and Cyanine 5 (Cy5), marked as single-stranded DNA (ssDNA), were synthesized by HITGEN (Chengdu, China). DOX was purchased from Beyotime (Shanghai, China). PEG-modified GNRs were synthesized in Beijing Zhongkeleiming Daojin Technology Co., LTD., through a two-step method. First, commercial gold seeds were synthesized via reducing $HAuCl_4$ solution using $AgNO_3$. Then, gold seeds were slowly crystallized into rod-shaped nanostructures in $HAuCl_4$ solution, after which PEG was coated at the surfaces of obtained GNRs. Tris-HCl, $MgCl_2$, and other chemicals were purchased from Aladdin (Shanghai, China).

Assembly of GNR-based Nanocomposites

In synthesizing TNDs, four 1-μL specific single-stranded DNA (detailed sequences are listed in Table 1) were equally mixed with 96 μL of TM buffer (10 mmol/L Tris, 10 mmol/L $MgCl_2$; pH = 8.0) and then heated to 95 °C. After being heated for 10 min at 95 °C, the solution containing DNA nanostructures was quickly cooled to 4 °C for 20 min. When preparing Cy5-labeled TDN, S1 strands were replaced by Cy5-S1 strands. Excessive DOX was incubated with the obtained TDNs (1 μmol/L) at 4 °C overnight to obtain TDN-DOX nanocomposites. Then, Tris-HCl, $MgCl_2$, and excessive DOX were removed by ultrafiltration centrifugation using 30-kD ultrafiltration cubes. Based on the synthesis protocol in the previous report[31], individual designed TDN nanostructure following provided design can carry 20 DOX molecules, showing a high loading ability. Then the obtained GNR was mixed with TDN-DOX nanocomplex to form GNR@TDN-DOX nanocomposites with different concentrations such as 1, 2, 3, 4, and 5 nmol/L. Then, the product was stored at 4 °C for the following experiment.

Characterization Techniques

Polyacrylamide gel electrophoresis (PAGE; 8%) was used to examine the synthesis of TDN, TDN@DOX nanocomposites, and GNR@TDN-DOX nanocomposites. Dynamic light scattering (DLS) was used to examine the hydrated particle size of the obtained nanocomposites. Transmission electron microscopy (TEM, FEI Tecnai F20 and Talos F200S G2, operated at 200 KV) was applied to investigate the specific structures and morphology of the obtained nanocomposites. TEM specimens of TDN

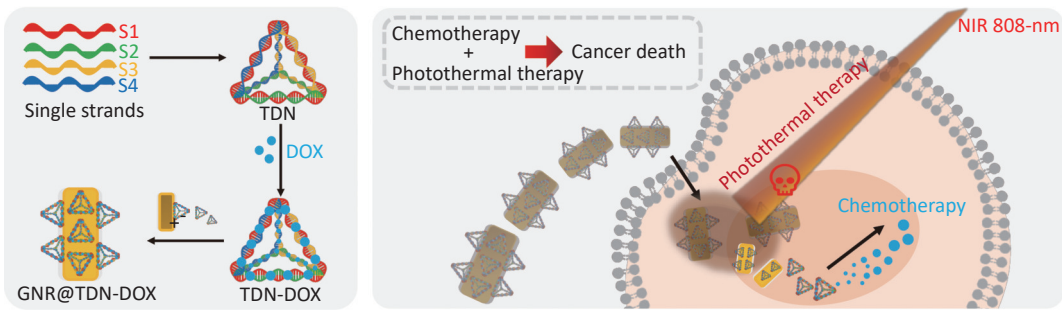

Figure 1. Schematic illustration for the assembly of GNR@TDN-DOX nanocomposites and the mechanism of combined chemo-photothermal therapy.

Table 1. Sequences of single-stranded DNA for the synthesis of TDNs

SsDNA	Direction	Sequence
S1	5′ to 3′	ATTTATCACCCGCCATAGTAGACGTATCACCAGGCAGTTGAGACGAACATTCCAAGTCTGAA
S2	5′ to 3′	ACATGCGAGGGTCCAATACCGACGATTACAGCTTGCTACACGATTCAGACTTAGGAATGTTCG
S3	5′ to 3′	ACGGTATTGGACCCTCGCATGACTCAACTGCCTGGTGATACGAGGATGGGCATGCTCTTCCCCG
S4	5′ to 3′	ACGGTATTGGACCCTCGCATGACTCAACTGCCTGGTGATACGAGGATGGGCATGCTCTTCCCG
Cy5-S1	5′ to 3′	cy5-ATTTATCACCCGCCATAGTAGACGTATCACCAGGCAGTT GAGACGAACATTCCTAAGTCTGAA

and TDN-DOX were negatively stained by 5% phosphotungstic acid-staining solution for 4 min before loading into TEM. UV–vis absorption curves were measured to analyze the optical characteristics of the obtained nanostructures.

Photothermal Measurements

GNRs and GNR@TDN-DOX nanocomposite solutions (1 nmol/L) were irradiated by 808-nm laser at a power density of 1.0, 1.5, and 2.0 W/cm^2, respectively, for 10 min. The temperature difference was measured by using a thermocouple thermometer at time intervals of 30 s. The temperature difference in three cycles of heating and cooling was measured to test the photothermal stability of the obtained nanostructures.

Cell Culture

Cells were seeded in culture dishes and cultivated in Dulbecco's modified Eagle's medium (DMEM) with 10% fetal bovine serum (FBS) and 1% penicillin streptomycin with an atmosphere of 5% CO_2 at 37 °C.

MTT Assay

A total of 2 × 10^4 L929 cells and A375 cells were seeded in 96-well plates and cultured overnight. Then, the cells were incubated with GNRs, DOX, TDN-DOX, and GNR@TDN-DOX solutions. The concentrations of GNR and GNR@TDN-DOX solutions were set as 1 nmol/L, with identical concentrations of DOX were adopted in DOX, TDN-DOX and GNR@TDN-DOX experimental groups. All groups of A375 cells were either treated with 808-nm laser irradiation of 2.0 W/cm^2 for 10 min or untreated. Then, the cells were cultured for 24 h, and their cell viability was analyzed by MTT assay.

Confocal Imaging Analysis of Cellular Uptake and Lysosomal Escape Ability

A375 cells were seeded in culture dishes as nanocomposites at 2 × 10^4 cells per well and cultivated overnight in DMEM with 10% FBS and 1% penicillin streptomycin at 37 °C with 5% CO_2. Then, the cells were incubated with GNRs, DOX, Cy5-labeled TDN-DOX, and Cy5-labeled GNR@TDN-DOX nanoparticles for 4 h. The concentrations of GNR and GNR@TDN-DOX solutions were set as 1 nmol/L, with identical concentrations of DOX were adopted in DOX, TDN-DOX and GNR@TDN-DOX experimental groups. For the cellular uptake study, the cells were stained with Hoechst solution. Then, the cells were washed with PBS three times. For lysosomal escape experiments, the cells were stained by lyso-linkers and Hoechst, after which the cells were washed with PBS three times. The fluorescence of cells was observed by using a fluorescence microscope (CLSM).

RESULTS

Advanced Characterization of TDN-DOX Nanocomposites

TDN was synthesized using four specific DNA base sequences (Table 1). Then, it was mixed with DOX to prepare DOX-loaded TDN nanoparticles, namely, TDN-DOX nanocomposites. The successful synthesis of TDN and TDN-DOX nanocomposites is shown in Figure 2. As shown in Figure 2A, four ssDNA evidently show high purity[32-34]. Notably, the TDN-DOX nanocomposite exhibits a slower immigration rate compared with TDN, which has a molecular weight of 200 bp, indicating that a high density of DOX has been attached to TDN. The single peak observed indicates the high purity of TDN-DOX. In addition, high-resolution TEM images were used to directly observe the morphology and geometry of TDN and the obtained TDN-DOX. Figure 2B and Figure 2C show the negatively stained TEM image of TDN and obtained TDN-DOX, respectively, showing a significantly different size. As shown in Figure 2D, DLS measurement was performed to quantitively understand the size change after loading DOX onto TDN, and the result indicates that the loading of DOX has significantly increased the size of TDNs from ~10 to ~20 nm, which further verifies the strong binding between DNA and DOX[35]. In addition, the sizes of these two nanostructures are consistent with the sizes measured by TEM. UV–vis absorption spectra of TDN and TDN-DOX were measured to verify the formation of TDN-DOX. The result shows that TDN only presents the DNA peak located at ~260 nm, whereas a peak presenting DOX at ~500 nm can be observed in TDN-DOX. Therefore, based on the abovementioned experimental results and analysis, the successful synthesis of TDN-DOX can be confirmed.

Advanced Characterization of GNR@TDN-DOX Nanocomposites

A thin PEG layer with positive charges and a nominal thickness of ~0.5 nm was prepared onto the GNRs to provide attachment sites for TDN-DOX on the surfaces of GNRs. In examining the binding ability between PEG-modified GNRs (namely, GNRs) and

TDN-DOX, a series of specimens with different GNR:TDN-DOX molar ratios (1:5, 1:10, 1:20, 1:50, and 1:100) was prepared. Figure 3A shows the electrophoretic band of GNR@TDN-DOX with different ratios and TDN. Using the band of TDN-DOX as a reference, when the molar ratio exceeds 1:10, unreacted TDN-DOX can be clearly observed, indicating that an individual GNR can be integrated with approximately 10 TND-DOX nanostructures. UV–vis absorption spectra measurement was conducted onto GNR@TDN-DOX with different GNR:TDN-DOX molar ratios to understand if the coupling of TND-DOX onto GNRs can affect the optical characteristics of GNR. As shown in Figure 3B, the integration between GNRs and TDN-DOX cannot significantly alter the optical characteristics of GNRs. In retaining a high thermal/heat conversion efficiency, the ratio between GNRs and TDN-DOX (1:5) was selected in the following cell experiments, considering the size of TDN-DOX. Furthermore, DLS was performed to examine the size difference between GNRs and GNR@TDN-DOX. As shown in Figure 3C, the size of GNRs was significantly increased by the addition of TDN-DOX nanocomposites. In understanding the structural characteristics of GNRs and GNR@TDN-DOX, systematic TEM investigations were performed. Figure 3D shows the low-magnification TEM of GNRs, displaying a uniform rod-like morphology. GNRs have a diameter of ~20 nm and a length of ~80 nm, leading to a length/diameter ratio of ~4 and corresponding to the observed absorption peak located at ~810 nm[36]. The insets of Figure 3E show the high-resolution TEM image of GNRs, with a lattice spacing of 0.2 nm, which corresponds to the {002} plane of gold. As {*00l*}(*l* = 1, 2, 3…n), where n is an integer, has the lowest surface energy in a face-centered cubic structure[37-40], the growth of the <001> direction is preferred in the formation of used GNR, leading to the uniform morphology and optical characteristics observed. As marked in Figure 3E, an ultrathin PEG layer can be observed at the surfaces of GNR. By contrast, Figure 3F shows the low-magnification TEM of GNR@TDN-DOX nanocomposites (GNR:TDN = 1:10, as an example for TEM characterization). The formed GNR@TDN-DOX nanocomposites process a thick and

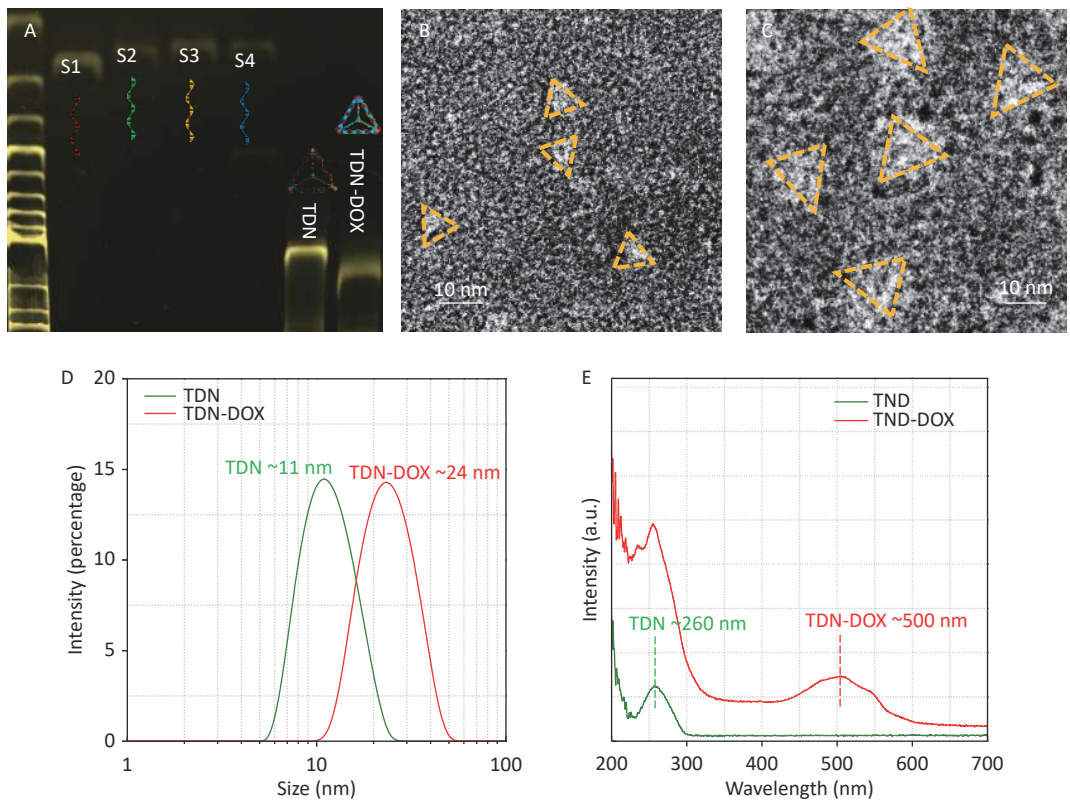

Figure 2. Characterization of TDN and TDN-DOX nanostructures: (A) PAGE analysis of four ssDNA, TDN, and TDN-DOX; (B) TEM image of TDN; (C) TEM image of TDN-DOX. (D) Size distribution of TDN and TDN-DOX measured by DLS. (E) UV–vis absorption spectra of TDN and TDN-DOX.

electron-transparent layer at the GNR surface, indicating that organic substances have been successfully coated on the surfaces of GNR, which can be confirmed as TDN-DOX based on the presented synthesis design. Figure 3G shows an enlarged TEM image of an individual GNR@TDN-DOX nanostructure, in which the outer layer can be clearly seen. Thus, GNR@TDN-DOX comprising GNRs as core and TDN-DOX as outer structures have been successfully fabricated.

Evaluation of Photothermal Performance of GNR@TDN-DOX Nanocomposites

In investigating the photothermal conversion ability of synthesized GNR@TDN-DOX nanocomposites, the heating temperature curves of GNRs and GNR@TDN-DOX at a concentration of 1.0 nmol/L were measured under 808-m NIR laser, with a power density of 1.0, 1.5, and 2.0 W/cm^2. Figure 4A shows the photothermal heating curves of GNRs, GNR@TDN-DOX nanocomposites, and water under 808-nm laser irradiation at a power density of 1.0, 1.5, and 2.0 W/cm^2, respectively, with irradiation duration of 10 min. The temperature of water only increases from ~25 °C to ~27 °C, indicating that this irradiation condition cannot damage the cells. GNR@TDN-DOX (1.0 nmol/L) displays a rapid heating rate, exceeding 45 °C in ~200 s at a power density of 2.0 W/cm^2. Based on previous studies, tumor cells can be effectively eliminated when the temperature is above 45 °C[41]. The GNR@TDN-DOX shows a good performance in the PTT. Interestingly, the maximum temperature of GNR@TDN-DOX was ~48 °C, which is slightly lower than that of GNRs at the same solution concentration, indicating that the TDN-DOX nanostructures anchored on the surface of GNRs gradually modulate the photothermal conversion ability of GNR. The photothermal stability of photothermal agents is another important factor influencing the PTT. The photothermal cycle heating curves of GNRs and GNR@TDN-DOX under 808-nm laser irradiation at a power density of 2.0 W/cm^2 for 10 min was measured to comprehensively understand the influence of the presence of TDN-DOX on the photothermal ability of GNR. As shown in Figure 4B, in three cycles, the maximum temperature of GNRs decreased significantly, which can result from the melting of GNRs under long-term irradiation[42].

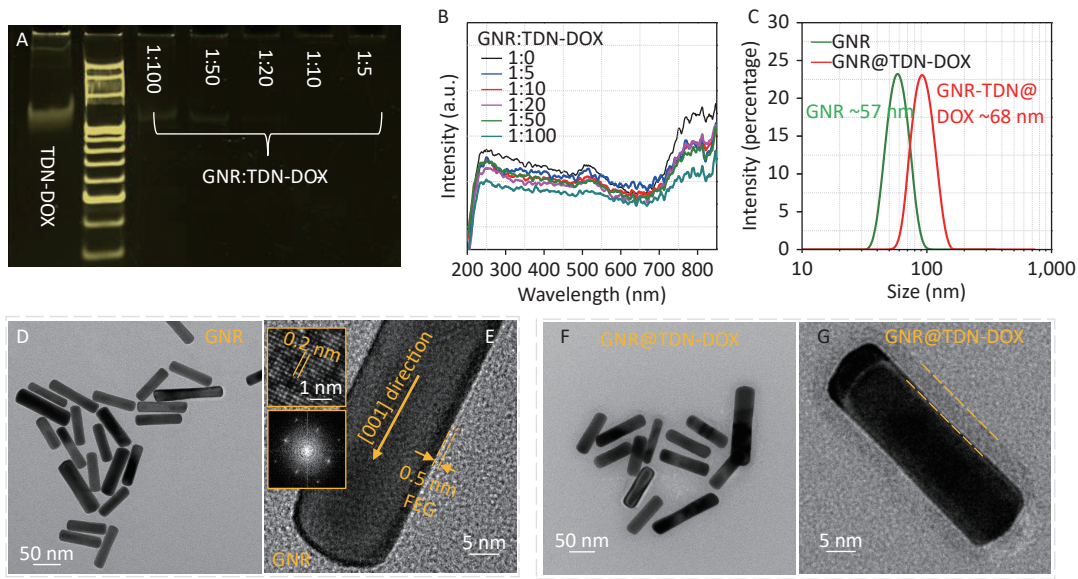

Figure 3. Characterization of GNRs and GNR@TDN-DOX nanocomposites: (A) PAGE analysis of TDN-DOX and GNR@TDN-DOX with a GNR:TDN-DOX molar ratio of 1:5, 1:10, 1:20, 1:50, and 1:100. (B) UV–vis absorption spectra of GNRS and GNR-DOX nanocomposites, with a GNR:TDN-DOX molar ratio of 1:5, 1:10, 1:20, 1:50, and 1:100. (C) Hydrated particle sizes of TDN and TDN-DOX measured by DLS. (D) Low-magnification TEM image of GNRs treated with a thin PEG layer. (E) High-magnification TEM image of PEG-modified GNRs (namely, GNRs), insets showing the atomic lattices and corresponding fast Fourier transform image. (F) Low-magnification TEM image of GNRs decorated with TDN-DOX, showing the core–shell structure. (G) High-magnification TEM image of GNRs decorated with TDN-DOX, with the outer nanostructures marked.

Moreover, the maximum temperature of GNR@TDN-DOX displays high stability in the heating and cooling cycles. Thus, TDN-DOX addition can effectively retain the photothermal stability of GNR because of the core–shell structure, providing a protective layer that favors practical tumor treatment. Figure 4C shows the maximum temperature of GNRs and GNR@TDN-DOX at a power density of 1.0, 1.5, and 2.0 W/cm^2. In this study, considering that the concentration is only at 1 nmol/L, modulating the concentration of GNR@ TDN-DOX can achieve a high temperature in the PTT.

In Vitro Cytotoxicity

In examining the biocompatibility of the obtained GNR@TDN-DOX nanocomposites, the cytotoxicity of TDN-DOX, DOX, GNRS, and GNR@TDN-DOX against L929 cells was estimated using MTT assay. Figure 5A shows *in vitro* cell viability of L929 cells treated with TDN-DOX, DOX, GNRs, and GNR@TDN-DOX. The concentrations of GNR and GNR@TDN-DOX solutions were set as 1 nmol/L, with identical concentrations of DOX were adopted in DOX, TDN-DOX and GNR@TDN-DOX experimental groups. GNR@TDN-DOX nanocomposites exhibit good biocompatibility based on the observed high cell viability.

In investigating the antitumor effects of TDN-DOX, DOX, GNRs, and GNR@TDN-DOX against A375 tumor cells, the live/dead cytotoxicity assay of TDN-DOX, DOX, GNRs, and GNR@ TDN-DOX under 808-nm laser irradiation at a power density of 2.0 W/cm^2

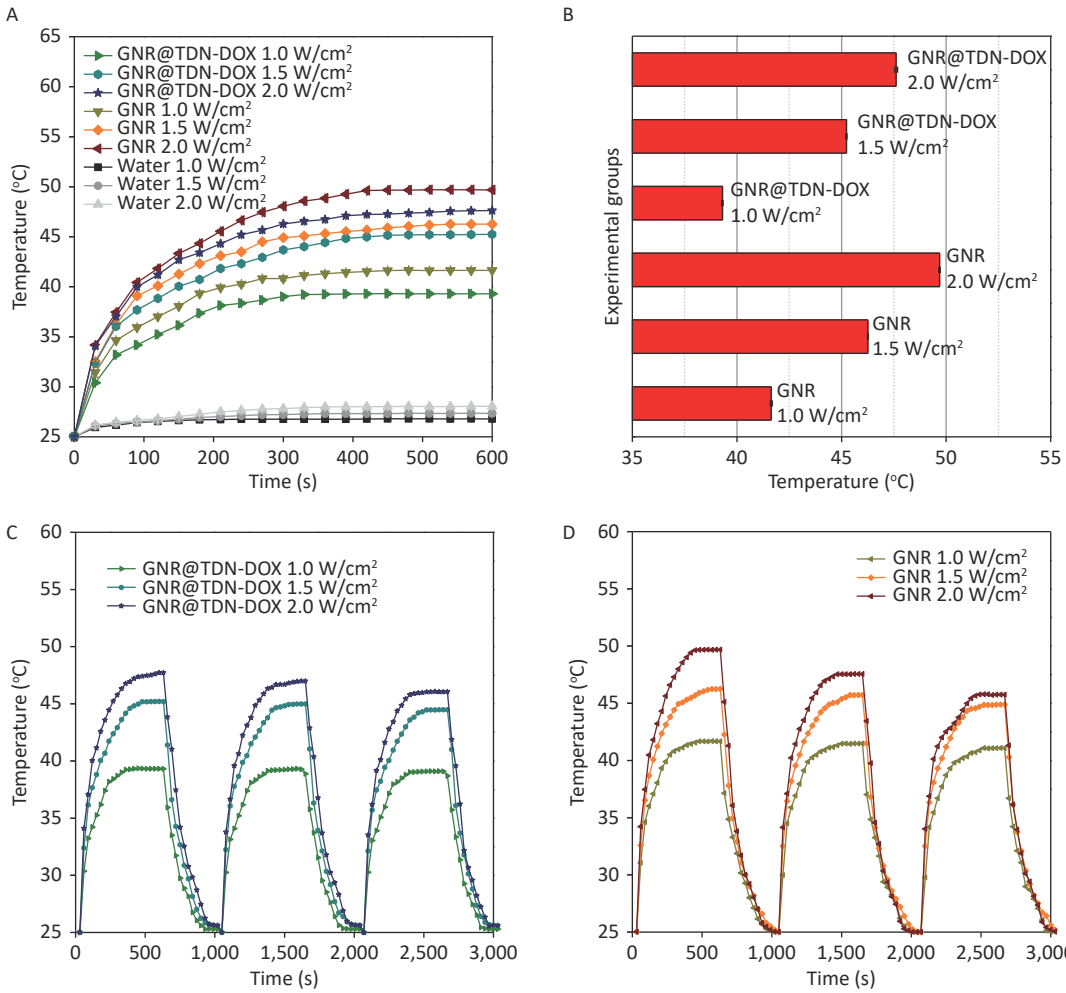

Figure 4. (A) Photothermal heating curves of GNR, GNR@TDN-DOX, and water under 808-nm laser irradiation at a power density of 1.0, 1.5, and 2.0 W/cm^2, respectively, for 10 min. (B) (C, D) Photothermal cycle heating curves of GNRS and GNR@TDN-DOX under 808-nm laser irradiation at a power density of 2.0 W/cm^2 for 10 min, indicating the photothermal stability. The temperature difference was measured every 30 s.

for 10 min was performed using the MTT method. As shown in Figure 5B, GNR@TDN-DOX nanocomposites exhibit the strongest antitumor performance among all the experimental groups, including the free chemotherapy group (DOX) and PTT group (GNR).

Cellular Uptake and Lysosome Escape

In comprehensively understanding the underlying mechanism of the effective antitumor effect of GNR@TDN-DOX, the cellular uptake behavior of GNR@TDN-DOX in A375 cells was further studied. First, after incubation with GNR@TDN-DOX for 4, 8, and 12 h, Figure 6A shows the cellular uptake of GNR@TDN-DOX in A375 cells observed by immunofluorescence staining. For microscopic observation, the nucleus of A375 cells was stained using Hoechst (blue), and GNR@TDN-DOX nanocomposites were labeled by Cy5. As shown in Figure 6A, after 4-h incubation, GNR@TDN-DOX nanocomposites (red fluorescence)

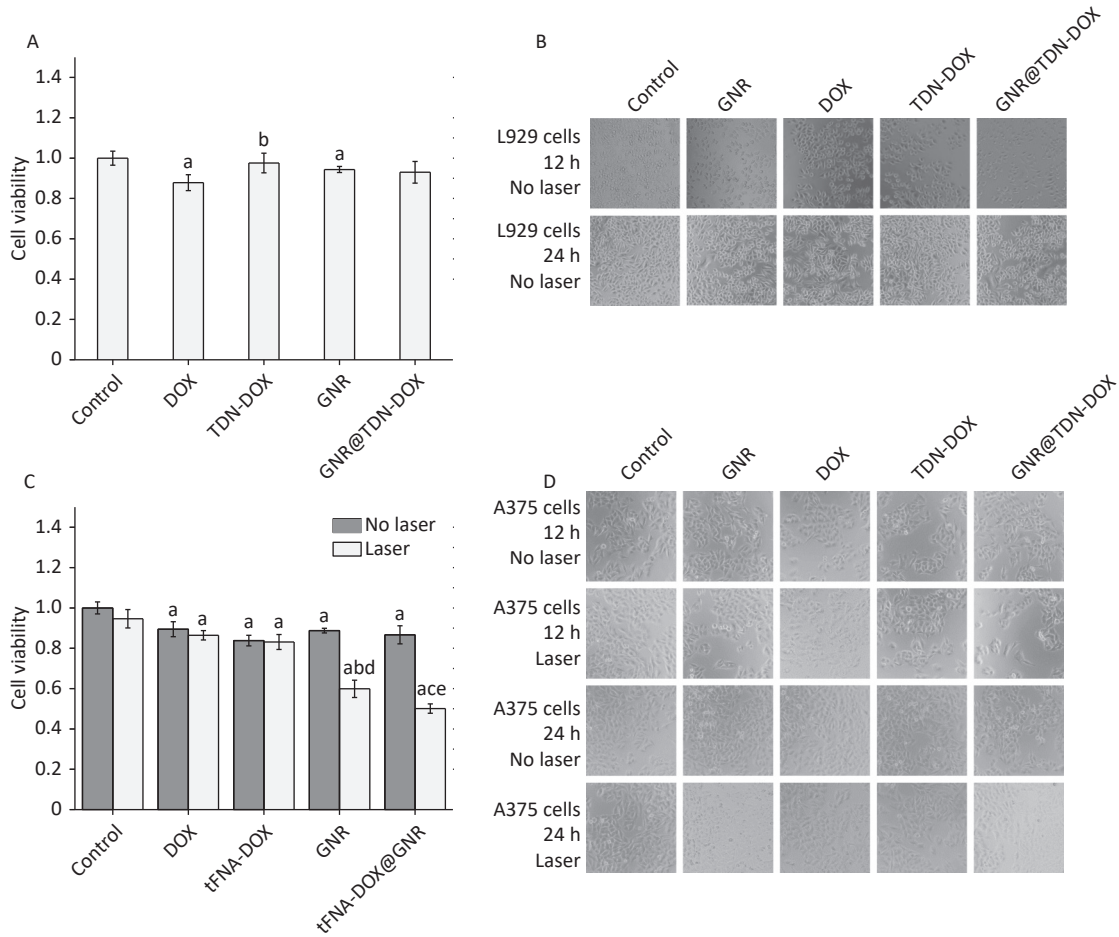

Figure 5. (A) *In vitro* cell viability of L929 cells treated with TDN-DOX, DOX, GNRs, and GNR@TDN-DOX tested by MTT assay. a presents statistical significance compared with the control group ($P < 0.05$); b presents statistical significance compared with the DOX group ($P < 0.05$). (B) Corresponding optical microscopy images of (A) when the incubation time was 12 and 24 h. (C) *In vitro* cell viability of A375 cells treated with TDN-DOX, DOX, GNRs and GNR@TDN-DOX tested by MTT assay, with/without laser irradiation at a power density of 2.0 W/cm^2 for 10 min. a presents statistical significance compared with the control group ($P < 0.05$); b presents statistical significance compared with the control group ($P < 0.05$). c presents statistical significance compared with DOX, TDN-DOX and GNR groups ($P < 0.05$); d presents statistical significance compared with GNR group without laser irradiation ($P < 0.05$); e presents statistical significance compared with GNR@TDN-DOX group without laser irradiation ($P < 0.05$). (D) Corresponding optical microscopic images of (C) with an incubation time of 12 and 24 h. All images were obtained under same magnification.

can be observed at the perinuclear region. Then, when the incubation time was extended to 8 h, a clear tendency of the GNR@TDN-DOX entering the nucleus can be observed. When the incubation time was extended to 12 h, a large amount of GNR@TDN-DOX nanocomposites entered the cell nucleus. This observation indicates that GNR@TDN-DOX nanocomposites have efficient cellular uptake and nuclear targeting functions.

Based on previous reports, TDN, a component of the GNR@TDN-DOX nanocomposites, can be decomposed by lysosomes[19]. Thus, investigating the intercellular behavior of GNR@TDN-DOX nanocomposites in A375 cells is necessary. Therefore, the lysosomal escape ability of Cy-5-labeled GNR@TDN-DOX nanocomposites was investigated through immunofluorescence staining. Figure 6B shows the fluorescence colocation of red (GNR@TDN-DOX labeled by Cy5) and green fluorescence (Lyso-trackers Green). After coincubation for 4, 8, and 12 h, the yellow fluorescence, which can be generated through the overlapping of green and red fluorescence, was very weak in A375 cells treated with GNR@TDN-DOX, revealing the lysosomal escape of GNR@TDN-DOX. Thus, GNR@TDN-DOX comprised GNRs, and TDN-DOX nanostructures successfully escaped from lysosomes and entered the nucleus, which can directly deliver antitumor drugs entering the nucleus and promote the antitumor performance.

DISCUSSION

The systematic study on the antitumor effect of obtained GNR@TDN-DOX nanocomposites indicates that they can achieve a synergistic antitumor effect. Through detailed experiments, the observed synergistic antitumor effect of GNR@TDN-DOX nanocomposites can be attributed to the effective drug delivery achieved by TDN as a media structure to carry DOX molecule and GNR nanostructures as the base in cellular uptake and provide photothermal heating, leading to cell cytotoxicity.

As witnessed, in the *In vitro* experiments, the low performance when applying free DOX indicates that a nanomaterial-based drug delivery system can promote tumor treatment using molecular drugs. The observed functions of obtained GNR@TDN-DOX nanocomposites are consistent with the advanced characterization results and photothermal heating analysis. As the release amount of DOX can be controlled by the TDN attached to GNR, further optimizing the molar ratio between GNRs and TDN-DOX can provide GNR@TDN-DOX nanocomposites with enhanced anticancer efficiency, suggesting the freedom in tuning the performance and components of designed nanocomposites. In addition, in the biosafety test, it was found that the cell viability of the TDN-DOX group is higher than the free DOX molecule group, indicating that the improvement of biocompatibility in this system can be attributed to the involvement of TDN nanostructures, which consist of non-toxic DNA. Thus, based on the abovementioned systematic investigation, GNR@TDN-DOX nanocomposites under 808-nm laser irradiation can generate a high-temperature local environment, which causes tumor cell death

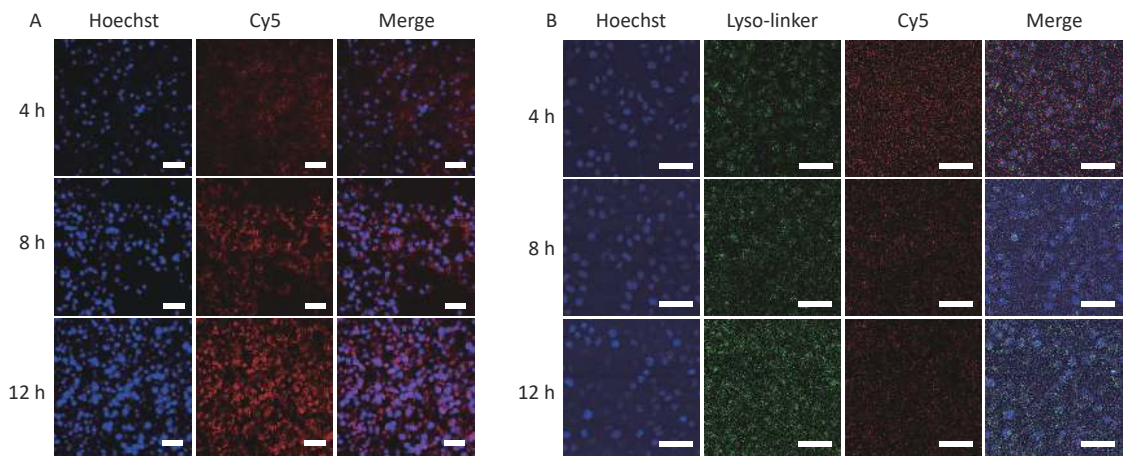

Figure 6. (A) Cellular uptake of GNR@TDN-DOX in A375 cells by immunofluorescence staining observed using CLSM (nuclear, blue; Cy5-labeled GNR@TDN-DOX, red) and (B) lysosomal escape ability of GNR@TDN-DOX in A375 cells by immunofluorescence staining observed using CLSM (nucleus, blue; Cy5-labeled GNR@TDN-DOX, red; lysosome, green). Scalebars are 75 μm in (A) and 50 μm in (B).

and chemotherapeutics by delivering DOX.

To comprehensively understand the advantages of GNR@TDN-DOX nanocomposites, it should be noted that GNR@TDN-DOX nanocomposites have efficient cellular uptake and nuclear targeting functions. As DOX primarily acts on the topoisomerase II within the nucleus and intercalates into DNA to cause cell apoptosis, the ability of GNR@TDN-DOX nanocomposites to enter the nucleus can directly provide DOX to inhibit DNA/RNA replication and attack the nucleus through photothermal heating, which can significantly cause tumor cell death. In addition, as the three-dimensional TDN nanostructures are comprised of DNA nanostructures, whose stability is sensitive to the temperature, the release of DOX can be enhanced under the irradiation condition, which can effectively induce the chemical therapy. Moreover, lysosomal escape is another key factor for nanomedicines in realizing their antitumor performance, the observed lysosomal escape of GNR@TDN-DOX nanocomposites can result from the surface characteristics of GNR@TDN-DOX nanocomplexes with a thin PEG decorated on the surfaces of GNRs.

In conclusion, in this work, a new nanoplatform for chemo-photothermal combination therapy through an assembly of PEG-modified GNRs and DOX-loaded TDN was developed. The successful synthesis of GNR@TDN-DOX nanocomposites was investigated by various advanced characterization techniques, indicating their application potential as an antitumor agent. The detailed experimental results indicate the GNR@TDN-DOX nanocomposites under NIR irradiation can induce severe apoptosis of cancer cells because of the synergistic effect caused by the effective PTT of GNRs, as well as the chemotherapy caused by the introduction of DOX. Furthermore, the GNR@TDN-DOX nanocomposites exhibit efficient cellular uptake and lysosomal escape ability, indicating their ability to enter the nucleus. Thus, the designed GNR@TDN-DOX nanocomposites, as a novel type of multifunctional nanomaterials, provide a new strategy for efficient tumor therapy. This strategy can be applied to other disease treatments, promoting the application of nanotechnology in bioscience and medical science.

AUTHOR CONTRIBUTIONS

WU Hao, as the first author, designed the experiment, conducted the experiment, and drafted the manuscript. GUO Bin and SUN Qiang, as corresponding authors, supervised the project. Other authors assisted with the experiment and revised the manuscript.

ACKNOWLEDGMENTS

The authors would like to express sincere thanks to all authors who helped complete this paper.

CONFLICTS OF INTEREST

All authors declare no conflicts of interest.

Received: October 14, 2022;
Accepted: November 15, 2022

REFERENCES

1. Miranda-Filho A, Bray F. Global patterns and trends in cancers of the lip, tongue and mouth. Oral Oncol, 2020; 102, 104551.
2. Vanshika S, Preeti A, Sumaira Q, et al. Incidence of HPV and EBV in oral cancer and their clinico-pathological correlation- a pilot study of 108 cases. J Oral Biol Craniofac Res, 2021; 11, 180−4.
3. Zhang Q, Hou D, Wen XY, et al. Gold nanomaterials for oral cancer diagnosis and therapy: advances, challenges, and prospects. Mater Today Bio, 2022; 15, 100333.
4. Zheng WP, Zhou QH, Yuan CQ. Nanoparticles for oral cancer diagnosis and therapy. Bioinorg Chem Appl, 2021; 2021, 9977131.
5. Wu WB, Shi LL, Duan YK, et al. Nanobody modified high-performance AIE photosensitizer nanoparticles for precise photodynamic oral cancer therapy of patient-derived tumor xenograft. Biomaterials, 2021; 274, 120870.
6. Ma CC, Wang ZL, Xu T, et al. The approved gene therapy drugs worldwide: from 1998 to 2019. Biotechnol Adv, 2020; 40, 107502.
7. Gao G, Sun XB, Liang GL. Nanoagent-promoted mild-temperature photothermal therapy for cancer treatment. Adv Funct Mater, 2021; 31, 2100738.
8. Lv ZQ, He SJ, Wang YF, et al. Noble metal nanomaterials for NIR-triggered photothermal therapy in cancer. Adv Healthc Mater, 2021; 10, 2001806.
9. Jia J, Liu GY, Xu WJ, et al. Fine-tuning the homometallic interface of Au-on-Au nanorods and their photothermal therapy in the NIR-II window. Angew Chem Int Ed, 2020; 59, 14443−8.
10. Wang S, Hu TT, Wang GY, et al. Ultrathin $CuFe_2S_3$ nanosheets derived from CuFe-layered double hydroxide as an efficient nanoagent for synergistic chemodynamic and NIR-II photothermal therapy. Chem Eng J, 2021; 419, 129458.
11. Zhao YN, Zhao TY, Cao YN, et al. Temperature-sensitive lipid-coated carbon nanotubes for synergistic photothermal therapy and gene therapy. ACS Nano, 2021; 15, 6517−29.
12. Wang C, Xu LG, Liang C, et al. Immunological responses triggered by photothermal therapy with carbon nanotubes in combination with anti-CTLA-4 therapy to inhibit cancer metastasis. Adv Mater, 2014; 26, 8154−62.
13. Song JB, Yang XY, Jacobson O, et al. Sequential drug release and enhanced photothermal and photoacoustic effect of hybrid reduced graphene oxide-loaded ultrasmall gold nanorod vesicles for cancer therapy. Acs Nano, 2015; 9,

9199−209.
14. Yin DY, Li XL, Ma YY, et al. Targeted cancer imaging and photothermal therapy via monosaccharide-imprinted gold nanorods. Chem Commun (Camb), 2017; 53, 6716−9.
15. Gao NY, Chen Y, Li L, et al. Shape-dependent two-photon photoluminescence of single gold nanoparticles. J Phys Chem C, 2014; 118, 13904−11.
16. Ding L, Yao CJ, Yin XF, et al. Size, shape, and protein corona determine cellular uptake and removal mechanisms of gold nanoparticles. Small, 2018; 14, 1801451.
17. Liu XY, Wang JQ, Ashby CR Jr, et al. Gold nanoparticles: synthesis, physiochemical properties and therapeutic applications in cancer. Drug Discov Today, 2021; 26, 1284−92.
18. Wu TT, Liu JB, Liu MM, et al. A nanobody-conjugated DNA nanoplatform for targeted platinum-drug delivery. Angew Chem Int Ed, 2019; 58, 14224−8.
19. Zhang T, Tian TR, Lin YF. Functionalizing framework nucleic-acid-based nanostructures for biomedical application. Adv Mater, 2021; 34, 2107820.
20. Zhang BW, Tian TR, Xiao DX, et al. Facilitating in situ tumor imaging with a tetrahedral DNA framework-enhanced hybridization chain reaction probe. Adv Funct Mater, 2022; 32, 2109728.
21. Li JJ, Yao YX, Wang Y, et al. Modulation of the crosstalk between schwann cells and macrophages for nerve regeneration: a therapeutic strategy based on a multifunctional tetrahedral framework nucleic acids system. Adv Mater, 2022; 34, 2202513.
22. Li SH, Liu YH, Zhang T, et al. A tetrahedral framework DNA-based bioswitchable miRNA inhibitor delivery system: application to skin anti-aging. Adv Mater, 2022; 34, 2204287.
23. Gao SJY, Li YJ, Xiao DX, et al. Tetrahedral framework nucleic acids induce immune tolerance and prevent the onset of type 1 diabetes. Nano Lett, 2021; 21, 4437−46.
24. Ma WJ, Yang YT, Zhu JW, et al. Biomimetic nanoerythrosome-coated aptamer-DNA tetrahedron/maytansine conjugates: pH-responsive and targeted cytotoxicity for HER2-positive breast cancer. Adv Mater, 2022; 34, 2109609.
25. Li J, Lai YX, Li MX, et al. Repair of infected bone defect with clindamycin-tetrahedral DNA nanostructure complex-loaded 3D bioprinted hybrid scaffold. Chem Eng J, 2022; 435, 134855.
26. Zhang M, Zhang XL, Tian TR, et al. Anti-inflammatory activity of curcumin-loaded tetrahedral framework nucleic acids on acute gouty arthritis. Bioact Mater, 2022; 8, 368−80.
27. Wang Y, Li YJ, Gao SJY, et al. Tetrahedral framework nucleic acids can alleviate taurocholate-induced severe acute pancreatitis and its subsequent multiorgan injury in mice. Nano Lett, 2022; 22, 1759−68.
28. Lin M, Wang JJ, Zhou GB, et al. Programmable engineering of a biosensing interface with tetrahedral DNA nanostructures for ultrasensitive DNA detection. Angew Chem Int Ed Engl, 2015; 54, 2151−5.
29. Sirong S, Yang C, Taoran T, et al. Effects of tetrahedral framework nucleic acid/wogonin complexes on osteoarthritis. Bone Res, 2020; 8, 6.
30. Liu MT, Ma WJ, Zhao D, et al. Enhanced penetrability of a tetrahedral framework nucleic acid by modification with iRGD for DOX-targeted delivery to triple-negative breast cancer. ACS Appl Mater Interfaces, 2021; 13, 25825−35.
31. Liu MT, Ma WJ, Li QS, et al. Aptamer-targeted DNA nanostructures with doxorubicin to treat protein tyrosine kinase 7-positive tumours. Cell Prolif, 2019; 52, e12511.
32. Zhang TX, Zhou M, Xiao DX, et al. Myelosuppression alleviation and hematopoietic regeneration by tetrahedral-framework nucleic-acid nanostructures functionalized with osteogenic growth peptide. Adv Sci, 2022; 9, 2202058.
33. Sun Y, Liu YH, Zhang BW, et al. Erythromycin loaded by tetrahedral framework nucleic acids are more antimicrobial sensitive against *Escherichia coli* (*E. coli*). Bioact Mater, 2021; 6, 2281−90.
34. Fu W, Ma L, Ju Y, et al. Therapeutic siCCR2 loaded by tetrahedral framework DNA nanorobotics in therapy for intracranial hemorrhage. Adv Funct Mater, 2021; 31, 2101435.
35. Zang YD, Wei YC, Shi YJ, et al. Chemo/photoacoustic dual therapy with mRNA-triggered DOX release and photoinduced shockwave based on a DNA-gold nanoplatform. Small, 2016; 12, 756−69.
36. Yang W, Xia B, Wang L, et al. Shape effects of gold nanoparticles in photothermal cancer therapy. Mater Today Sustainability, 2021; 13, 100078.
37. Wallenberg LR, Bovin JO, Schmid G. On the crystal structure of small gold crystals and large gold clusters. Surf Sci, 1985; 156, 256−64.
38. Sun Q, Gao H, Zhang XT, et al. Free-standing InAs nanobelts driven by polarity in MBE. ACS Appl Mater Interfaces, 2019; 11, 44609−16.
39. Sun Q, Gao H, Yao XM, et al. Au-catalysed free-standing wurtzite structured InAs nanosheets grown by molecular beam epitaxy. Nano Res, 2019; 12, 2718−22.
40. Sun Q, Pan D, Li M, et al. *In situ* TEM observation of the vapor-solid-solid growth of <00$\bar{1}$> InAs nanowires. Nanoscale, 2020; 12, 11711−7.
41. Chen JQ, Ning CY, Zhou ZN, et al. Nanomaterials as photothermal therapeutic agents. Prog Mater Sci, 2019; 99, 1−26.
42. Taylor AB, Siddiquee AM, Chon JWM. Below melting point photothermal reshaping of single gold nanorods driven by surface diffusion. ACS Nano, 2014; 8, 12071−9.